Part X

Investigating Magnetospheric Processes

37

Global Simulations

Joachim Raeder[1], Kai Germaschewski[1], William D. Cramer[1], and John Lyon[2]

ABSTRACT

Over the past few decades global simulations have emerged as a valuable new tool to study the magnetosphere–ionosphere–thermosphere system, to the point where some of them are considered community models available for runs on demand by the community at the Community Coordinated Modeling Center (CCMC). Most leading global models are still based on the conventional and well-established MHD approximation; they are remarkably successful reproducing the major features and processes in geospace. Here, we briefly review the purpose and utility of such models, their history, their basic structure, the need for submodels of the ionosphere–thermosphere system and the inner magnetosphere, as well as inherent model limitations. The major computational and numerical constraints are discussed and recent simulations addressing plasma injections and sawtooth oscillations are presented.

37.1. PURPOSE AND UTILITY

The magnetosphere is a complex physical system, comparable in complexity to the atmosphere or the oceans. While the latter allow for comprehensive measurements, both with in situ and remote sensing approaches, measurements in the magnetosphere are difficult to obtain, because satellites are expensive and cannot be placed arbitrarily. There are only few possibilities for remote sensing known, such as Energetic Neutral Atom (ENA) imaging (Gruntman, 1997) and the so far unproven soft X-ray imaging (Sibeck et al., 2018). Also, the ionosphere can act to some extent as a projection screen for magnetospheric processes (Mende, 2016a, 2016b); however, such projections may be difficult to interpret and may be misleading.

Because of the magnetosphere's complexity, analytical solutions are virtually impossible to come by and numerical approaches are required. The analogy to the atmosphere and the oceans holds here too, as the study of these natural systems also heavily relies on numerical modeling.

Such global models of the magnetosphere or the entire geospace, that is, including the ionosphere and the thermosphere as well, serve a number of purposes:

- The models encode our basic understanding of the physical processes that govern the magnetosphere. Besides numerical limitations, the models solve the physical processes as we understand them. Any discrepancies between the model results and observations may then point to a particular lack of our understanding, apart from the possibility that the model input is wrong. As an example, very early in the global modeling efforts it became clear that the coupling with the ionosphere–thermosphere system is essential to understand magnetospheric dynamics.
- The models allow us to conduct numerical experiments. Because of the vastness of the magnetosphere, laboratory experiments are not possible, with few exceptions, such as "terella" experiments (Rypdal and Brundtland, 1997) and plasma chamber experiments of localized phenomena such as Alfvèn waves and magnetic reconnection (Gekelman et al., 2011; Olson et al., 2016). With models,

[1]*Space Science Center, University of New Hampshire, Durham, NH, USA*

[2]*Department of Physics and Astronomy, Dartmouth College, Hanover, NH, USA*

Space Physics and Aeronomy Collection Volume 2: Magnetospheres in the Solar System, Geophysical Monograph 259, First Edition.
Edited by Romain Maggiolo, Nicolas André, Hiroshi Hasegawa, and Daniel T. Welling.

DOI: 10.1002/9781119815624.ch37

it is possible to vary parameters or switch off certain feedbacks to investigate the effects. That allows, even in a complex system, a more reductionist approach to be applied to study the phenomena.

• Although there are now dozens of spacecraft probing the magnetosphere, it is still vastly undersampled. Together with the dynamic nature of the magnetosphere, it is often difficult to interpret the observations and to put them into context. For example, an early use of a global model helped interpret observations from the distant magnetotail that were at the time controversial (Frank et al., 1995). Likewise, simulations addressing the very first GEM (NSF's Geospace Environment Program) challenge (Lyons, 1998) helped clarify open questions about the open–closed boundary for a specific event.

• Global simulations can help with the planning of missions. Because of orbital constraints it is impossible to place satellites at ideal sampling locations. Instead, one must strive to find orbits that maximize the dwell time in the places that one wishes to sample most densely. Such planning was done, for example, for a magnetosphere constellation mission, which still has to materialize (Raeder and Angelopoulos, 1998).

• Finally, global models can serve as the starting point for operational geospace forecast models. It may seem that a geospace model may be used as a forecast model per se. However, forecasts impose additional requirements, such as robustness and the ability to tolerate erroneous inputs. Also, "science grade" models are often not well documented (because grants generally do not support that) and can often only be effectively used by their creators and their collaborators. By contrast, an operational model must be independent from their developers and not require any more continuous developer support.

Historically, the first models in the United States were developed at NRL (Brecht, 1985; Brecht et al., 1981, 1982; Fedder and Lyon, 1987) and at UCLA (Leboeuf et al., 1978; Ogino, 1986). In the early 1990s the National Science Foundation (NSF) Geospace Environment Modeling (GEM) program commenced, with the stated goal to develop one or more community models of the geospace system. It was originally envisioned that such models would comprise a collection of coupled models for various regions, such as bow shock, magnetosheath, lobes, etc. However, it was quickly realized that such an approach would not be practical. At the same time, better computer resources and better algorithms made the existing MHD-based models more and more realistic, and doubts about the limitations of MHD faded. The early GEM challenges (Lyons, 1998; Raeder and Maynard, 2001) were essentially a turning point that established the MHD models as "spines" that were subsequently complemented by coupling them to ionosphere–thermosphere models and models of the inner magnetosphere. The UCLA model eventually developed into the OpenGGCM (Raeder, 2003; Raeder et al., 2008), while the NRL model became the LFM (Lyon et al., 2004). In the early 2000s the BATS-R-US model became another major global model of the magnetosphere (Powell et al., 1999), which developed into the Space Weather Modeling Framework (Tóth et al., 2005). During the same time frame the GUMICS model (Janhunen et al., 2012) was developed in Europe. Many more global models were developed over the years; however, these four models stand out because they are available as community models at the Community Coordinate Modeling Center (ccmc.gsfc.nasa.gov). At the CCMC any user can request model runs on demand for these models, and the CCMC also provides a number of analysis and visualization tools.

37.2. GOVERNING EQUATIONS, INITIAL AND BOUNDARY CONDITIONS

Ideally, the magnetosphere is described by Maxwell's equations for the fields and Boltzmann equations for the various plasma species. Since the magnetosphere plasma can be assumed collisionless, the Boltzmann equations can be replaced by Vlasov equations. However, this set of equations cannot be easily solved numerically, because the fastest timescale, given by the plasma frequency, is too fast, and the smallest spatial scale that needs to be numerically resolved, the Debye length, is too small to be properly resolved numerically. Thus, most contemporary global magnetosphere models are based on the ideal magnetohydrodynamic (MHD) equations, which have no intrinsic spatial scale, and the timescales are given by the system size and wave speeds. Here, "ideal" means that there are no explicit dissipation terms in the equations. As we shall see, however, the numerical solutions always contain dissipation. The MHD equations are discussed in more detail in Chapter 3 of this volume; however, for the purpose of global modeling some specific issues must be addressed.

The MHD equations can be written in various forms, which are all mathematically equivalent. However, when it comes to solving them numerically, their form matters. For reasons outlined below, the fully conservative form is preferable, but sometimes not practical. One therefore often uses a semiconservative form that solves for the plasma energy density $U = \rho v^2/2 + p/(\gamma - 1)$ instead of the total energy density $e = \rho v^2/2 + p/(\gamma - 1) + B^2/2\mu_0$. The latter can be problematic where the plasma β ($=2\mu_0 p/B^2$) is low, and therefore the pressure p becomes the difference of two large numbers, which leads to large errors. Here, γ is the adiabatic constant, p is the pressure, ρ the plasma density, and B the magnetic field.

For a mathematically well posed problem, proper initial and boundary values must also be specified. There is no good analytic equilibrium solution of the magnetosphere suitable as an initial condition. One therefore starts with a dipole embedded in more or less uniform plasma representing the solar wind. That may seem trivial but is not. First, the velocity field must be tapered to zero near the Earth, because otherwise the dipole would just get blown away. Also, the near Earth region within 2–4 R_E (the MI coupling region) is usually treated differently, and the MHD equations are not solved there. Furthermore, since the dipole field is cut off at the boundaries of the simulation box, Maxwell's law $\nabla \cdot \mathbf{B} = 0$ would be violated at the boundaries. That is not much of a problem at the outflow boundaries, because erroneous fields would be convected away, but is problematic at the inflow boundary. A proper initial condition can be obtained by using a mirror dipole, as explained in detail in Raeder (2003).

The simulation domains generally have three different types of boundaries. On the sunward side all characteristics point inward, and thus Dirichlet conditions are required. These can be artificial values for the IMF and the solar wind, but often these boundary conditions are taken from SW/IMF measurements upstream of the Earth. Here, a difficulty arises because one usually only has a point measurement, which also may be far upstream of the Earth. However, one needs to specify boundary values on the entire inflow boundary. A simple solution involves ballistic propagation of the measured values with the ambient solar wind speed to the boundary, and some sort of extrapolation of that point value across the entire boundary.

An additional difficulty arises at the inflow boundary due to the $\nabla \cdot \mathbf{B} = 0$ constraint, which implies that across discontinuities $\mathbf{n} \cdot (\mathbf{B}_{\text{upstream}} - \mathbf{B}_{\text{downstream}}) = 0$. Thus, if one simply extrapolates the point measurement, one implicitly assumes that the normal $\mathbf{n}$ points sunward, implying that B_x can never change. A possible solution is to find the predominant normal vector $\mathbf{n}$ in the sense that all solar wind discontinuities during some time period are only a function of $\mathbf{n}$. This is difficult with a single solar wind monitor; however, boundary normal methods (for example, the minimum variance method (Sonnerup and Cahill, 1967, 1968)) can be applied. After $\mathbf{n}$ is found, one transforms the IMF time series into the minimum variance coordinates, sets B_n to either zero or an appropriate average value, and transforms back (Raeder et al., 1998). The values on the inflow face must then be set accordingly to the assumed sheet structure of the solar wind, i.e., constant on the planes perpendicular to $\mathbf{n}$. Using this procedure, the steadiness of B_n provides a quality indicator. If B_n varies much, this is simply an indicator that the solar wind structure is not sheath like but more convoluted. In that case, one can often not do much except for setting the IMF B_x to zero with the assumption the B_x has the least influence on magnetosphere dynamics.

The lateral and the back boundary are easier to treat. Here, one usually assumes a "free flow" boundary, that is, all variable normal derivatives are set to zero. Because of $\nabla \cdot \mathbf{B} = 0$ this should only be applied to the transverse field components, and the normal component derivative is then given by the divergence constraint. Strictly speaking, such a boundary condition does not guarantee free outflow, because it can still reflect waves. However, it works satisfactorily as long as the back boundary is within supermagnetosonic flow. In practice this means that the back boundary must be several hundred R_E behind Earth. Likewise, the lateral boundaries are placed far enough away so as to not perturb the simulation near the Earth. In practice, that distance is some 20–50 R_E on either side of the Earth.

A boundary also exists at the earthward side of the simulation. There, the MHD solution connects with ionosphere dynamics, as discussed further below in section 37.4.

37.3. NUMERICAL APPROACHES AND THEIR LIMITATIONS

Constructing a numerical model of the magnetosphere that solves the MHD equations, or a similar set of fluid and field equations, starts with a discretization algorithm and an associated numerical grid. Some possible choices for grids are depicted in Figure 37.1. The simplest choice would be a uniform Cartesian grid (Figure 37.1a). However, it is easy to see that if such a grid were to cover the entire magnetosphere, while providing good resolution in critical regions, such as at the magnetopause, one would need of the order of 10^9 grid cells. Such a grid would not be computationally efficient. With a stretched Cartesian grid (Figure 37.1b) the efficiency improves by about two orders of magnitude, while an adapted spherical or cylindrical grid (Figure 37.1c), an Adaptive Mesh Refinement (AMR) grid (Figure 37.1d), or a tetrahedral grid (Figure 37.1e) can be even more efficient. However, the more complex grids incur other computational costs as well as more complex algorithms that require more manpower to develop. Simulations with poor resolution (of the order of 0.3–0.5 R_E) are possible and potentially useful, for example, for very long time periods where higher resolution would incur prohibitive computational costs. At such resolution, the bow shock, magnetopause, tail plasma sheet, and boundary layers are just barely resolved. Currently, models are run with typical resolution of 0.1–0.3 R_E near the Earth, which is sufficient for many studies. However, simulations with very good

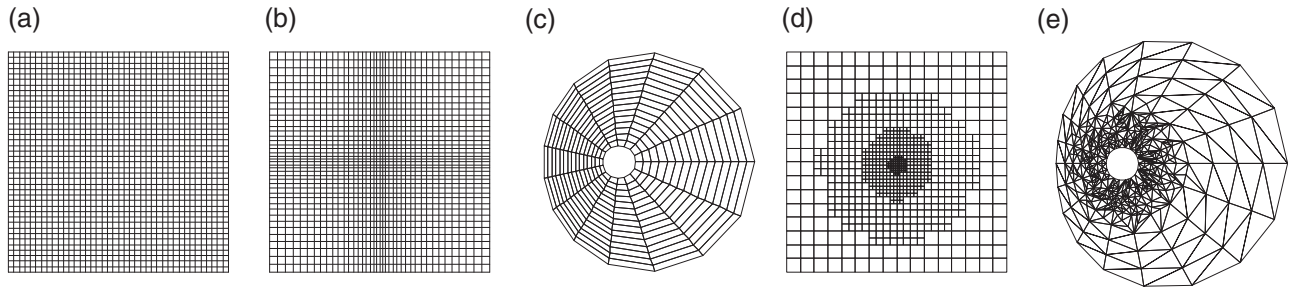

Figure 37.1 Several common choices for numerical grids: (a) a uniform Cartesian grid, (b) a stretched Cartesian grid, (c) a non-Cartesian grid with Cartesian topology, (d) a structured adaptive grid, (e) an unstructured grid.

resolution (of the order of the ion skin depth, ~100 km) have also been performed (Dorelli et al., 2007; Wiltberger et al., 2015). Although the MHD approximation is no longer valid at or below the ion skin depth scale, such extremely high resolution simulations may still make sense, because the high resolution also reduces numerical diffusion.

All of the grid types shown in Figure 37.1 have been used for global magnetosphere models, for example by Ogino (1986) (Cartesian), Raeder (1995) and Raeder et al. (1995) (stretched Cartesian), Lyon et al. (2004) (adapted spherical or cylindrical grid), Janhunen et al. (2012) and Powell et al. (1999) (AMR), and Tanaka (1995) (tetrahedral).

With the grid comes a numerical discretization of the equations, i.e., the continuous functions are represented by a finite number of values located on the spatial grid and in time. For the spatial discretization, most models use Finite Difference (FD) or Finite Volume (FV) methods (see Hirsch (1990) and Laney (1998), for example). The derivatives are replaced by discrete equations that link neighboring grid points or grid cells, both in space and time.

The time derivative is usually discretized with a scheme that is at least second order accurate, i.e., the associated errors are of the order of Δt^2, where Δt is the time step. That ensures that the solution converges as $\Delta t \to 0$. Typical choices are a predictor-corrector type scheme, or a second order Runge–Kutta scheme (Hirsch, 1990). A simpler first order algorithm would not be sufficient, because the global solution to a given time T requires $N = T/\Delta t$ steps, so that the accumulated error would not decrease. A tradeoff exists between explicit and implicit time stepping schemes. The former are easy to implement and require much less computation. However, they are only conditionally stable, that is, the solution becomes unstable if the time step is too large. Specifically, the stability criterion is given by $\Delta t < \alpha h/v_{\max}$, where h is the size of the grid cells, $v_{\max}$ the largest speed in the system, i.e., magnetosonic speed plus flow speed, and α is a constant of the order of one, which depends on the specific algorithm. This criterion is known as the Courant–Fridrichs–Levy (CFL) criterion and can be very restrictive for magnetosphere simulations, because the Alfvén speeds are large close to Earth. A remedy, employed by most global models is the so-called Boris correction (Boris, 1970), by keeping the displacement current part of the MHD equations. That re-introduces electromagnetic waves and the light speed c into the equations. One can then set c to an artificially low value and thereby limit all wave speeds without significantly affecting the solutions (Brecht, 1985).

The CFL criterion gives rise to the first law of global MHD simulations:

> *The computational cost of a simulation rises as $h^{-(d+1)}$, where h is the smallest grid spacing and d is the number of spatial dimensions, i.e., it rises as h^{-4} for three-dimensional simulations.*

Thus, there is a severe penalty to double the resolution, because a finer grid also requires a smaller time step. On the flip side, increasing h, even by a rather small amount, can make simulation runs significantly faster. At the time of writing, all major codes can be run with modest computational resources and reasonable grids ($h \sim 0.2\ R_E$) faster than real time, i.e., the wall clock time is smaller than the simulated time period. This is a prerequisite for using the models in an operational setting for space weather forecasting. It is also encouraging to compare the above law with Moore's law, which says that the transistor count on semiconductor circuits, and thus the computing power, roughly doubles every 18 months (Schaller, 1997). Fortunately, that exponential growth outpaces the power law of simulation cost, that is, the feasible h should be decreasing faster and faster in time as long as Moore's law holds.

The spatial derivatives are usually also discretized by finite differences, if the grid is sufficiently regular, or with a finite volume method if the grid has more complicated cells, such as the grids (c) and (e) shown in Figure 37.1. FV methods are a generalization of FD methods, and most FV methods reduce to a known FD method if the grid is Cartesian. Replacing the differentials with discrete

FD equations, such as $\partial U(x)/\partial x|_i \approx (U_{i+1} - U_{i-1})/2h$, appears to be simple but leads to disastrous results. Here, U is a variable, i a grid index, and h the grid spacing. In reality, the Taylor series that lead to the difference equations are truncated, and therefore the FD equations incur error terms that are proportional to the higher derivatives of the solution U. The error terms that are proportional to the odd derivatives introduce artificial dispersion, and the terms associated with even derivatives create artificial diffusion. If the solutions are sufficiently smooth, the error terms may be of minor importance, because smooth solutions have limited higher derivatives (see, for example, Sod (1985), Hirsch (1990), Laney (1998) or other numerical analysis texts for a discussion of FD error terms). However, the magnetosphere is characterized by the presence of shocks and discontinuities. At discontinuities, the higher order derivatives have no bounds and the error terms dominate. With symmetric FD such as the one shown before, the dispersive errors dominate and create growing oscillations at discontinuities, which lead to instability. Smooth solutions can be obtained by using FD equations where the even error term dominates, such as one-sided FD equations (a.k.a. "upwind schemes"), the Lax scheme, or the Rusanov scheme (Laney, 1998). While these schemes can provide smooth solutions, they are unacceptably diffusive, i.e., discontinuities smear out excessively and the diffuse terms in Faraday's law represent finite resistivity.

The quest for numerical schemes that properly resolve discontinuities has been central to the applied mathematics and engineering disciplines for decades, because the same problems arise, for example, in supersonic gas flow, transport equations, and traffic flow equations. Such schemes are called "shock capturing schemes," and they are discussed in many textbooks, for example Hirsch (1990) or Laney (1998). Such schemes are known as "Flux Corrected Transport" (FCT), "Total Variance Diminishing" (TVD), or "Weighted Essentially Nonoscillatory" (WENO) schemes, for example. They all have in common that they use more accurate high order schemes in regions where there are no discontinuities, but introduce diffusion at discontinuities to counteract the dispersive errors that would destroy the solution near discontinuities. Local numerical diffusion at discontinuities is virtually impossible to avoid. However, on a global scale diffusion typically decreases as a function of grid spacing like h^{-n}, where n is typically larger than two. This gives rise to the second law of global MHD simulations:

> *There exists no numerical scheme that truly solves the ideal MHD, or similar nondiffusive equations. All stable schemes are dominated by diffusion at discontinuities, but overall diffusion depends on the grid and decreases as h^{-n}, with $n \geq 2$.*

The consequences for global magnetosphere simulations are:

- It is impossible to suppress magnetic reconnection (see Gonzalez and Parker (2016) for a discussion of the topic). The magnetosphere, like almost all systems in space plasmas (solar corona, heliosphere), tends to produce current sheets, which are numerically discontinuities. These may have a tendency to become tearing unstable, even if they would be stable in reality. The good news is that the reconnection rates, in nature, as in the simulations, tend to be around the canonical value of 1/10 (Cassak et al., 2017).
- Discontinuities tend to smear out. This is less so for shocks, because the shock physics (which is correctly captured by the models) keeps a shock steepening until other processes limit the gradients within a shock. However, other discontinuities, in particular tangential and rotational discontinuities, tend to broaden with time. Therefore, boundary layers are difficult to resolve properly.
- Simulations are always a compromise between the first and the second law, both in the design of the algorithms and in the choice of grids for individual simulations.
- For a long time to come, global simulations will require the most computational power available, just as, for example, weather or climate forecasts.

37.4. COUPLING WITH THE IONOSPHERE–THERMOSPHERE SYSTEM

Very early MHD models of the magnetosphere had essentially no coupling with an ionosphere. The ionosphere was simply mimicked by a highly diffusive region within a few R_E of Earth (Ogino and Walker, 1984; Winglee, 1994). It was soon realized, however, that the inclusion of at least an electrodynamical model of the ionosphere was critical (Fedder and Lyon, 1987) to account for magnetosphere–ionosphere (MI) coupling. The theory of the electrodynamical magnetosphere–ionosphere coupling had been laid out earlier (Vasyliunas, 1970; Wolf, 1975, 1983). The coupling arises from the fact that the magnetosphere generates field-aligned currents, which flow into the ionosphere and need to close there. The closure occurs through horizontal ionospheric (Pedersen) currents that are controlled by the finite conductance of the ionosphere plasma due to collisions with the neutral thermosphere (Kelly, 2009). The current closure creates an electric potential, which can be obtained with the solution of a potential equation:

$$\nabla \cdot \underline{\underline{\Sigma}} \cdot \nabla \Phi = -j_{\parallel} \sin I.$$

Here, Φ is the ionosphere potential, $\underline{\underline{\Sigma}}$ the conductance tensor, $j_{\parallel}$ is the field-aligned current (FAC) entering the ionosphere, and I is the field line inclination. In this context, the ionosphere is generally assumed to be a

two-dimensional entity, because the conductance along field lines is very high even in the collisional ionosphere, and thus field lines can be considered equipotentials. This is no longer true in mid and low latitudes where the field lines are more inclined. However, at these latitudes, the field lines are closed and map close to the earth. This region is not directly driven by the solar wind interaction, but rather from the dynamics within the ionosphere, such as the equatorial electrojet.

Since the field lines are to a good approximation equipotentials, the ionosphere controls the magnetosphere convection. Two extreme cases are possible. If the ionosphere conductance is zero, no currents can flow into the ionosphere. Therefore, the currents must close somewhere above the ionosphere, and the ionosphere cannot affect convection. Since the ionosphere is always a sink of electrodynamic energy coming from the magnetosphere (Strangeway and Raeder, 2001), magnetosphere convection is then inhibited as little as possible by the ionosphere. In the other extreme, ionosphere conductance is infinite, i.e., the ionosphere is a superconductor. Then, Φ and the convection electric field are zero, and magnetosphere convection is eventually shut down. This was demonstrated by Raeder et al. (1996) with global simulations. In reality, the situation lies somewhere in between these two extremes. As a consequence there is significant Poynting flux from the magnetosphere into the ionosphere (Knipp et al., 2011; Li et al., 2011).

A key element of the the ionosphere potential equation above is the conductance tensor $\underline{\underline{\Sigma}}$, which is made up of the Hall and Pedersen conductances (Kelly, 2009). Early models used either a constant conductance or a simple analytical model for the conductance. However, this generally leads to unsatisfactory results (Raeder et al., 2001a, 2001b), since conductance gradients can skew the convection patters (Atkinson and Hutchison, 1978) and because the pattern of empirical conductance models does not match the patterns of the currents. The dayside conductance is dominated by solar EUV radiation, while the nightside conductance is dominated by precipitating electrons (Hardy et al., 1987). The dayside conductance therefore has mostly solar cycle, seasonal, and diurnal variations, while the nightside conductance is highly variable. The variation of conductance can substantially influence magnetosphere dynamics (Jensen et al., 2017).

Most global models are therefore coupled with an ionosphere–thermosphere model, which provides more realistic conductances. With such coupling, the MHD equations are not solved within about 2–3 R_E of earth. Instead, the field-aligned currents are mapped from that inner boundary into the ionosphere. In addition, electron precipitation is calculated using empirical formulas (Raeder, 2003). These parameters are then fed into a fully dynamic ionosphere–thermosphere model. In the case of the OpenGGCM, this is the NOAA CTIM model (Fuller-Rowell et al., 1996), and the LFM is coupled with a version of the TIE-GCM ionosphere code (Wang et al., 2004).

Another form of MI coupling occurs through the outflow of ionospheric plasma into the magnetosphere. This plasma consists of protons and heavy ions such as O^+ and molecular ions (Poppe et al., 2016; Strangeway, 2005) and can affect magnetosphere dynamics, for example, by changing the mass density and rates of magnetic reconnection. Such outflow has been incorporated into some global models, along with a multifluid extension to MHD (Brambles et al., 2011; Glocer et al., 2009).

37.5. COUPLING WITH INNER MAGNETOSPHERE MODELS

MHD is not a good approximation for the behavior of plasma in the inner magnetosphere, that is, the ring current and the radiation belts. Here, the plasma β is low, and the plasma dynamics is dominated by gradient and curvature drift, as opposed to plasma pressure and magnetic forces (Wolf, 1983). In parallel to the MHD models, models for the inner magnetosphere have been developed (Chapter 20, this volume). These inner magnetosphere (IM) models are based on a quasi-static approximation, i.e., they include no inertial terms, but they resolve particle energy and possibly also pitch angle (Fok and Moore, 1997; Kozyra et al., 1998; Toffoletto et al., 2004). They only solve the equations in a subset of the closed field line domain with simplified magnetic and electric fields. However, their plasma solutions (density and pressure) are considered to be more realistic than MHD, giving reason to combine MHD and IM models. On the one hand, IM models require the magnetic and electric fields, as well as boundary conditions that can be supplied by the MHD models. In reverse, the IM models can provide more realistic plasma pressure and density distribution for the inner magnetosphere compared to the MHD model. In practice, the simulation volumes of the IM and MHD model overlap in the regions of closed field lines where the IM models are valid. The models run in parallel, where the MHD model supplies the electric and magnetic fields, or related values, such as the flux tube volume. The MHD model also provides plasma parameters on the boundaries of the IM model. In return, the plasma pressure and density from the IM model is used by the MHD model to correct the MHD values in the region of overlap. In practice, this leads to the development of a ring current with realistic pressure and density, and a more realistic plasma drift. In addition, the IM model can also contain an electron fluid, which also calculates the proper drift physics, and can be used to calculate more

realistic electron precipitation in the region of closed field lines.

37.6. RECENT SIGNIFICANT RESULTS

Although contemporary global models are based on the rather simple MHD formalism, they have been remarkably successful in reproducing the basic morphology of the magnetosphere and many of the basic physical processes, for example, magnetopause reconnection (Berchem et al., 1995a, 1995b; Dorelli et al., 2004), Flux Transfer events (Raeder, 2006), the plasma depletion layer (Wang et al., 2003), plasma entry due to double lobe reconnection (Li et al., 2005, 2008, 2009), interplanetary shock impacts (Oliveira and Raeder, 2014), or magnetopause Kelvin–Helmholtz waves (Claudepierre et al., 2016).

Here, we present results from two contemporary models, the LFM and the OpenGGCM. The examples were chosen in the first case to demonstrate the realism of the simulations with respect to recent observations of plasma entry into the inner magnetosphere, and in the second case to demonstrate how the models can be exploited as a numerical laboratory to investigate fundamental physical processes.

37.6.1. Plasma Injection

It has been known for some time that plasma does not convect continuously from the tail into the inner magnetosphere, but rather in so-called Bursty Bulk Flows (BBFs) or bubbles with depleted entropy (Chapter 17, this volume). It has been an open question as to how BBFs are related to bubbles, how much they contribute to the plasma injected into the IM, and how deep these injections can penetrate.

In recent work (Cramer et al., 2017) we used the OpenGGCM coupled with the RCM to investigate these questions. Figure 37.2 shows the result from a geomagnetic storm simulation. The figure traces out the minima in flux tube entropy, i.e., bubbles, and maxima in flow velocity, i.e., BBFs. There is nearly a one-to-one correlation, around 70–80%, between these two quantities, tailward of 8 R_E. This correlation persists further inward towards the earth, but falls off to about 20% at 4 R_E. Comparing the plasma transport due to bubbles compared to steady convection shows that transport due to bubbles dominates all the way to about 4 R_E during storms. Comparison with a quiet time simulation shows that transport is very similarly dominated by bubbles tailward of 8 R_E but somewhat less closer to earth.

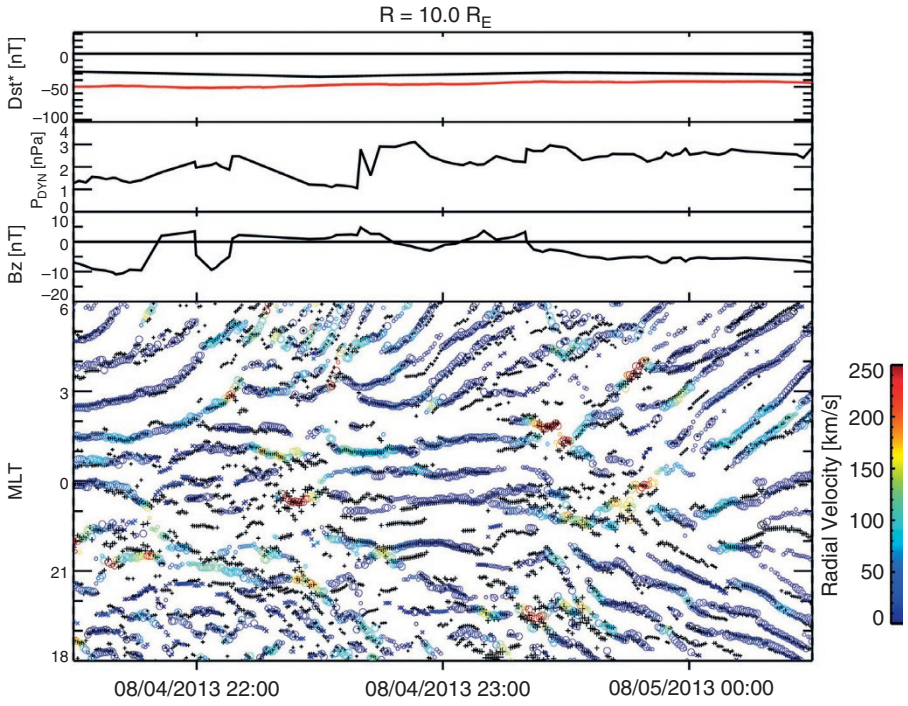

Figure 37.2 Time series of velocity maxima and flux tube entropy minima in the current sheet at 10 R_E during the main phase of a geomagnetic storm (I1). The panels show, from top to bottom: the Dst index (red for the simulation), the solar wind dynamic pressure, the IMF B_z, and a time–MLT diagram of bubbles (local entropy minima, + symbols), and BBFs (colored symbols, where the color represents the speed.)

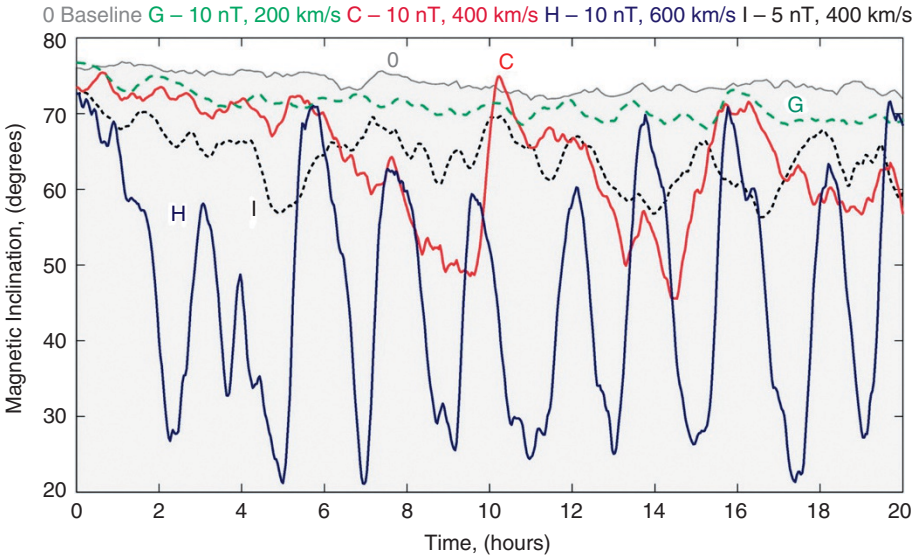

Figure 37.3 LFM simulation of sawtooth event and control simulations. The figure shows magnetic inclination angle as a function of simulation time near local midnight at geosynchronous altitude. The colors of the time traces correspond to the simulation parameters at the top of the figure. The blue line, representing a run with large negative IMF B_z and large solar wind speed, exhibits oscillations resembling sawtooth events, whereas the control runs do not. The figure is from Brambles et al. (2011).

37.6.2. Sawtooth Oscillations

Global sawtooth oscillations in the magnetosphere (Henderson et al., 2006) have been identified as large-scale plasma injections associated with dipolarizations of the inner magnetosphere magnetic field and auroral brightenings. They have a typical repetition period of 2–3 hours and have some characteristics of large substorms. They are typically associated with high-speed solar wind and extended periods of southward IMF.

Brambles et al. (2011) used multifluid LFM simulations with an empirical polar outflow model to study the magnetosphere response during solar wind conditions typical for sawtooth events and compared that run with simulations that had more benign solar wind conditions.

Figure 37.3 shows that the sawtooth run indeed produced sawtooth like oscillation in the near Earth plasma sheet, whereas the control runs did not produce such oscillations. Analysis of the simulation led the authors to conclude that ionosphere outflow of O^+ enhanced the plasma pressure in the tail and led to the periodic shedding of plasmoids with the characteristic sawtooth frequency.

ACKNOWLEDGMENTS

Work at UNH was supported by grant AGS-1603021 from the National Science Foundation, by grants NNX15AW16G, 80NSSC17K0720, and NNX13AK31G from the National Aeronautics and Space Administration, and by grant FA9550-18-1-0483 from the Air Force Office of Scientific Research.

REFERENCES

Atkinson, G., and Hutchison, D. (1978). Effect of the day night ionospheric conductivity gradient on polar cap convective flow. *J. Geophys. Res.*, 83, 725. doi:10.1029/ja083ia02p00725

Berchem, J., Raeder, J., and Ashour-Abdalla, M. (1995a). Magnetic flux ropes at the high-latitude magnetopause. *Geophys. Res. Lett.*, 22, 1189.

Berchem, J., Raeder, J., and Ashour-Abdalla, M. (1995b). Reconnection at the magnetospheric boundary: Results from global MHD simulations. In B. U. Sonnerup and P. Song (Eds.), *Physics of the magnetopause, Geophysical Monograph Series* (Vol. 90, p. 205). American Geophysical Union.

Boris, J. P. (1970). *A physically motivated solution of the Alfvèn problem, NRL memorandum report 2167*. Naval Research Laboratory, Washington, DC.

Brambles, O. J., Lotko, W., Zhang, B., Wiltberger, M., Lyon, J., and Strangeway, R. J. (2011). Magnetosphere sawtooth oscillations induced by ionospheric outflow. *Science*, 332(6034), 1183–1186. doi:10.1126/science.1202869.

Brecht, S. H. (1985). Global simulations using MHD codes: A few points to consider before you try one. *Space Sci. Rev.*, 42, 169.

Brecht, S. H., Lyon, J. G., Fedder, J. A., and Hain, K. (1981). A simulation study of east-west IMF effects on the magnetosphere. *Geophys. Res. Lett.*, 8, 397.

Brecht, S. H., Lyon, J. G., Fedder, J. A., and Hain, K. (1982). A time dependent three dimensional simulation of the Earth's

magnetosphere: Reconnection events. *J. Geophys. Res.*, 87, 6098.

Cassak, P. A., Liu, Y.-H., and Shay, M. A. (2017). A review of the 0.1 reconnection rate problem. *J. Plasma Phys.*, 83(5), 715830501.

Claudepierre, S. G., Toffoletto, F. R., and Wiltberger, M. (2016). Global MHD modeling of resonant ULF waves: Simulations with and without a plasmasphere. *J. Geophys. Res.*, 121, 227–244. doi:10.1002/2015ja022048.

Cramer, W. D., Raeder, J., Toffoletto, F. R., Gilson, M., and Hu, B. (2017). Plasma sheet injections into the inner magnetosphere: Two-way coupled OpenGGCM-RCM model results. *J. Geophys. Res.*, 122, 5077–5091. doi:10.1002/2017ja024104.

Dorelli, J. C., Hesse, M., Kuznetsova, M. M., Rastaetter, L., and Raeder, J. (2004). A new look at driven magnetic reconnection at the terrestrial subsolar magnetopause. *J. Geophys. Res.*, 109, A12216, doi:10.1029/2004JA010458.

Dorelli, J. C., Bhattacharjee, A., and Raeder, J. (2007). Separator reconnection at Earth's dayside magnetopause under generic northward interplanetary magnetic field conditions. *J. Geophys. Res.*, 112(A2).

Fedder, J. A., and Lyon, J. G. (1987). The solar wind–magnetosphere–ionosphere current-voltage relationship. *Geophys. Res. Lett.*, 14, 880.

Fok, M. C., and Moore, T. E. (1997). Ring current modeling in a realistic magnetic field configuration. *Geophys. Res. Lett.*, 24, 1775.

Frank, L. A., Ashour-Abdalla, M., Berchem, J., Raeder, J., Paterson, W. R., Kokubun, S., et al. (1995). Observations of plasmas and magnetic fields in Earth's distant magnetotail: Comparison with a global MHD model. *J. Geophys. Res.*, 100, 19177. doi:10.1029/95ja00571.

Fuller-Rowell, T. J., Rees, D., Quegan, S., Moffett, R. J., Codrescu, M. V., and Millward, G. H. (1996). A coupled thermosphere-ionosphere model (CTIM). In R. W. Schunk (Ed.), *Step report* (p. 217). NOAA/NGDC, Boulder, CO: Scientific Committee on Solar Terrestrial Physics (SCOSTEP).

Gekelman, W., Vincena, S., Compernolle, B. V., Morales, G. J., Maggs, J. E., Pribyl, P., and Carter, T. A. (2011). The many faces of shear Alfvén waves. *Phys. Plasmas*, 18, 055501. doi:10.1063/1.3592210.

Glocer, A., Toth, G., Gombosi, T., and Welling, D. (2009). Modeling ionospheric outflows and their impact on the magnetosphere, initial results. *J. Geophys. Res.*, 114. doi:10.1029/2009ja014053.

Gonzalez, W., and Parker, E. (2016). *Magnetic reconnection, Astrophysics and Space Science Library* (Vol. 427). Springer.

Gruntman, M. (1997). Energetic neutral atom imaging of space plasmas. *Rev. Sci. Instrum.*, 68, 3617–3656. doi:10.1063/1.1148389.

Hardy, D. A., Gussenhoven, M. S., Raistrick, R., and McNeil, W. J. (1987). Statistical and functional representations of the pattern of auroral energy flux, number flux, and conductivity. *J. Geophys. Res.*, 92, 12275.

Henderson, M. G., Reeves, G. D., Skoug, R., Thomsen, M. F., Denton, M. H., Mende, S. B., et al. (2006). Magnetospheric and auroral activity during the 18 April 2002 sawtooth event. *J. Geophys. Res.*, 111. doi:10.1029/2005ja011111.

Hirsch, C. (1990). *Numerical computation of internal and external flow* (Vol. II). John Wiley & Sons, Inc., New York.

Janhunen, P., Palmroth, M., Laitinen, T., Honkonen, I., Juusola, L., Facsko, G., and Pulkkinen, T. (2012). The GUMICS-4 global MHD magnetosphere-ionosphere coupling simulation. *J. Atmos. Sol.-Terr. Phys.*, 80, 48–59. doi:10.1016/j.jastp.2012.03.006

Jensen, J. B., Raeder, J., Maynard, K., and Cramer, W. D. (2017). Particle precipitation effects on convection and the magnetic reconnection rate in earth's magnetosphere. *J. Geophys. Res.*, 122, 11413–11427.

Kelly, M. C. (2009). *The Earth's Ionosphere*. Elsevier.

Knipp, D., Eriksson, S., Kilcommons, L., Crowley, G., Lei, J., Hairston, M., and Drake, K. (2011). Extreme Poynting flux in the dayside thermosphere: Examples and statistics. *Geophys. Res. Lett.*, 38. doi:10.1029/2011gl048302.

Kozyra, J. U., Fok, M.-C., Sanchez, E. R., Evans, D. S., Hamilton, D. C., and Nagy, A. F. (1998). The role of precipitation losses in producing the rapid early recovery phase of the great magnetic storm of February 1986. *J. Geophys. Res.*, 103, 6801.

Laney, C. B. (1998). *Computational gas dynamics*. Cambridge University Press.

Leboeuf, J. N., Tajima, T., Kennel, C. F., and Dawson, J. M. (1978). Global simulation of the time dependent magnetosphere. *Geophys. Res. Lett.*, 5, 609.

Li, W., Raeder, J., Dorelli, J., Øieroset, M., and Phan, T. D. (2005). Plasma sheet formation during long period of northward IMF. *Geophys. Res. Lett.*, 32, L12S08.

Li, W., Raeder, J., Dorelli, J. C., Thomsen, M., and Lavraud, B. (2008). Solar wind entry into the magnetosphere under northward IMF conditions. *J. Geophys. Res.*, 113, A04204.

Li, W., Raeder, J., Øieroset, M., and Phan, T. D. (2009). Cold dense magnetopause boundary layer under northward IMF: Results from THEMIS and MHD simulations. *J. Geophys. Res.*, 114, A00C15.

Li, W., Raeder, J., and Knipp, D. (2011). The relationship between dayside local Poynting flux enhancement and cusp reconnection. *J. Geophys. Res.*, 116, A08301.

Lyons, L. R. (1998). The geospace modeling program grand challenge. *J. Geophys. Res.*, 103, 14781–14785. doi:10.1029/98ja00015.

Lyon, J. G., Fedder, J. A., and Mobarry, C. M. (2004). The Lyon-Fedder-Mobarry (LFM) global MHD magnetospheric simulation code. *J. Atm. Sol.-Terr. Phys.*, 66, 1333.

Mende, S. B. (2016a). Observing the magnetosphere through global auroral imaging: 1. Observables. *J. Geophys. Res.*, 121, 10623–10637.

Mende, S. B. (2016b). Observing the magnetosphere through global auroral imaging: 2. Observing techniques. *J. Geophys. Res.*, 121, 10638–10660.

Ogino, T. (1986). A three dimensional MHD simulation of the interaction of the solar wind with the Earth's magnetosphere: The generation of field aligned currents. *J. Geophys. Res.*, 91, 6791.

Ogino, T., and Walker, R. J. (1984). A magnetohydrodynamic simulation of the bifucation of the tail lobes during intervals with a northward inter planetary magnetic field. *Geophys. Res. Lett.*, 11, 1018.

Oliveira, D. M., and Raeder, J. (2014). Impact angle control of interplanetary shock geoeffectiveness. *J. Geophys. Res.*, 119, 8188. doi:10.1002/2014JA020275.

Olson, J., Egedal, J., Greess, S., Myers, R., Clark, M., Endrizzi, D., et al. (2016). Experimental demonstration of the collisionless plasmoid instability below the ion kinetic scale during magnetic reconnection. *Phys. Rev. Lett.*, 116. doi:10.1103/physrevlett.116.255001.

Poppe, A. R., Fillingim, M. O., Halekas, J. S., Raeder, J., and Angelopoulos, V. (2016). ARTEMIS observations of terrestrial ionospheric molecular ion outflow at the moon. *Geophys. Res. Lett.*, 43, 6749–6758. doi:10.1002/2016gl069715.

Powell, K. G., Roe, P. L., Linde, T. J., Gombosi, T. I., and DeZeeuw, D. L. (1999). A solution-adaptive upwind scheme for ideal magnetohydrodynamics. *J. Comp. Phys.*, 154, 284.

Raeder, J. (1995). Global MHD simulations of the dynamics of the magnetosphere: Weak and strong solar wind forcing. In J. R. Kan, J. D. Craven, and S.-I. Aka- sofu (Eds.), *Proceedings of the second international conference on substorms* (p. 561).

Raeder, J. (2003). Global magnetohydrodynamics – A tutorial. In J. Buchner, C. T. Dum, and M. Scholer (Eds.), *Space plasma simulation, Lecture Notes in Physics Series* (Vol. 615, pp. 212–246). Springer Verlag.

Raeder, J. (2006). Flux transfer events: 1. Generation mechanism for strong southward IMF. *Ann. Geo.*, 24, 381.

Raeder, J., and Angelopoulos, V. (1998). Using global simulations of the magnetosphere for multi-satellite mission planning and analysis. In V. Angelopoulos and P. V. Panetta (Eds.), *Science closure and enabling technologies for constellation class missions* (p. 78). University of California, Berkeley, and NASA Goddard Space Flight Center.

Raeder, J., and Maynard, N. (2001). Foreword. *J. Geophys. Res.*, 106, 345.

Raeder, J., Walker, R. J., and Ashour-Abdalla, M. (1995). The structure of the distant geomagnetic tail during long periods of northward IMF. *Geophys. Res. Lett.*, 22, 349.

Raeder, J., Berchem, J., and Ashour-Abdalla, M. (1996). The importance of small scale processes in global MHD simulations: Some numerical experiments. In T. Chang and J. R. Jasperse (Eds.), *The physics of space plasmas* (Vol. 14, p. 403). Cambridge, MA.

Raeder, J., Berchem, J., and Ashour-Abdalla, M. (1998). The geospace environment modeling grand challenge: Results from a global geospace circulation model. *J. Geophys. Res.*, 103, 14787–14797. doi:10.1029/98ja00014.

Raeder, J., Larson, D., Li, W., Kepko, E. L., and Fuller-Rowell, T. (2008). Open-GGCM simulations for the THEMIS mission. *Space Sci. Rev.*, 141, 535.

Raeder, J., Wang, Y. L., and Fuller-Rowell, T. J. (2001a). Geomagnetic storm simulation with a coupled magnetosphere–ionosphere–thermosphere model. In P. Song, G. Siscoe, and H. J. Singer (Eds.), *Space weather, Geophysical Monograph Series* (Vol. 125, pp. 377–384). American Geophysical Union.

Raeder, J., Wang, Y. L., Fuller-Rowell, T. J., and Singer, H. J. (2001b). Global simulation of space weather effects of the Bastille Day storm. *Sol. Phys.*, 204, 325.

Rypdal, K., and Brundtland, T. (1997). The Birkeland terrella experiments and their importance for the modern synergy of laboratory and space plasma physics. *Le Journal de Physique IV*, C4–113–C4–132. doi:10.1051/jp4:1997408.

Schaller, R. R. (1997). Moore's law: past, present and future. *IEEE Spectrum*, 34(6), 52–59. doi:10.1109/6.591665.

Sibeck, D. G., Allen, R., Aryan, H., Bodewits, D., Brandt, P., Branduardi-Raymont, G., et al. (2018). Imaging plasma density structures in the soft X-rays generated by solar wind charge exchange with neutrals. *Space Sci. Rev.*, 214. doi:10.1007/s11214-018-0504-7.

Sod, G. A. (1985). *Numerical methods in fluid dynamics*. Cambridge University Press.

Sonnerup, B. U., and Cahill, L. J. (1967). Magnetopause structure and attitude from explorer 12 observations. *J. Geophys. Res.*, 72, 171. doi:10.1029/jz072i001p00171.

Sonnerup, B. U., and Cahill, L. J. (1968). Explorer 12 observations of the magnetopause current layer. *J. Geophys. Res.*, 73, 1757–1770. doi:10.1029/ ja073i005p01757.

Strangeway, R. J. (2005). Factors controlling ionospheric outflows as observed at intermediate altitudes. *J. Geophys. Res.*, 110. doi:10.1029/2004ja010829.

Strangeway, R. J., and Raeder, J. (2001). On the transition from collisionless to collisional magnetohydrodynamics. *J. Geophys. Res.*, 106, 1955.

Tanaka, T. (1995). Generation mechanisms for magnetosphere-ionosphere current systems deduced from a three-dimensional MHD simulation of the solar wind- magnetosphere-ionosphere coupling processes. *J. Geophys. Res.*, 100, 12057.

Toffoletto, F. R., Sazykin, S., Spiro, R. W., Wolf, R. A., and Lyon, J. G. (2004). RCM meets LFM: Initial results of one-way coupling. *J. Atm. Sol,-Terr. Phys.*, 66, 1361.

Toth, G., Sokolov, I. V., Gombosi, T. I., Chesney, D. R., Clauer, C. R., Zeeuw, D. L. D., et al. (2005). Space weather modeling framework: A new tool for the space science community. *J. Geophys. Res.*, 110. doi:10.1029/2005ja011126.

Vasyliunas, V. M. (1970). Mathematical models of magnetospheric convection and its coupling to the ionosphere. In B. M. McCormac (Ed.), *Particles and fields in the magnetosphere, Astrophysics and Space Science Library Series* (Vol. 17, pp. 60–71). D. Reidel, Dordrecht, The Netherlands.

Wang, W., Wiltberger, M., Burns, A., Solomon, S., Killeen, T., Maruyama, N., and Lyon, J. (2004). Initial results from the coupled magnetosphere–ionosphere–thermosphere model: thermosphere–ionosphere responses. *J. Atm. Sol.-Terr. Phys.*, 66, 1425–1441. doi:10.1016/j.jastp.2004.04.008.

Wang, Y. L., Raeder, J., Russell, C. T., Phan, T. D., and Manapat, M. (2003). Plasma depletion layer: Event studies with a global model. *J. Geophys. Res.*, 108. doi:10.1029/2002ja009281.

Wiltberger, M., Merkin, V., Lyon, J. G., and Ohtani, S. (2015). High-resolution global magnetohydrodynamic simulation of bursty bulk flows. *J. Geophys. Res.*, 120, 4555–4566.

Winglee, R. M. (1994). Non-MHD influences on the magnetospheric current system. *J. Geophys. Res.*, 99, 13437.

Wolf, R. A. (1975). Effects of ionospheric conductivity on convective flow of plasma in the magnetosphere. *J. Geophys. Res.*, 75, 4677.

Wolf, R. A. (1983). The quasi-static (slow flow) region of the magnetosphere. In R. L. Carovillano and J. M. Forbes (Eds.), *Solar terrestrial physics, Astrophysics and Space Science Library Series* (Vol. 104, pp. 303–368). Reidel, Hingham, MA.